nature communications

Article

https://doi.org/10.1038/s41467-025-61693-2

Biomimetic layered, ecological, advanced, multi-functional film for sustainable packaging

Received: 6 November 2024

Accepted: 26 June 2025

Published online: 19 July 2025

Check for updates

Puneet S. Dhatt[1,2], Acadia Hu[1], Cheng Hu[3,4], Vincent Huynh[1,2], Susie Y. Dai[2,3,4] & Joshua S. Yuan[1,2]

Plastic pollution is one of most daunting sustainability challenges. Multi-functional and biodegradable plastics are critical for both desirable end-of-life outcomes and petrochemical plastics replacement. Current bioplastics are either: short of mechanical properties, like polyhydroxybutyrate (PHB); lack room temperature biodegradability, like polylactic acid (PLA); or lack the functionality to create additional values. Here, we present the bioinspired Layered, Ecological, Advanced, and multi-Functional Film (LEAFF), for sustainable plastic packaging. This biomimetic composite, based on the structure of the natural plant leaf, synergistically improves mechanical strength while empowering PLA for rapid ambient soil biodegradability, achieving complete degradation in 5 weeks. The film is also highly transparent and water stable, and achieves high gas barrier properties to improve food shelf life and reduce waste. The biomimetic design showcases the synergistic advantage leveraged by the LEAFF's multilayer structure to enhance mechanical performance while simultaneously retaining biodegradability and achieving multifunctionality for broad applications.

Plastics are indispensable to the everyday functioning of the modern world. However, their ubiquitous use presents significant sustainability challenges due to their high carbon emissions and persistent environmental pollution[1–4]. Since their industrial adoption in 1950, plastic production has exponentially increased from 2Mt. in 1951 to over 459Mt. in 2019[5–7]. Globally, nearly half of all of the plastic waste generated annually is due to single-use plastic (SUP) packaging, the vast majority of which are not biodegradable[8]. Today, 91% of plastic waste is landfilled or incinerated, with only 9% being recycled[1]. This landfilled or incinerated waste fragments into microplastics that find their way into humans through our water, food, and air[8–11]. Consumption or inhalation of microplastics has been associated with increased risk for numerous pathologies such as cardiovascular and respiratory disease and lung cancer[10,12–15]. Additionally, non-degradable plastic waste finds its way into the world's waterways and oceans, severely negatively impacting marine life[2,7,16]. Even though recent policies advocate for interdictions on single-use plastic manufacturing, or seek to implement recycling programs for repurposing plastic packaging materials, these efforts are not effective due to low recovery rates[17,18]. Furthermore, it has been estimated that an SUP ban alone will not be enough to solve the plastic waste problem[18,19]. Thus, sustainable material alternatives are necessary to replace petroleum plastic use cases.

Today's $23.5 billion plastic packaging market is dominated by polyethylene and polypropylene, accounting for more than half of non-fiber plastic production[20]. These polymers are utilized for their high tensile strength (polyethylene: 20-45 MPa; polypropylene: 35 MPa) and water resistance[21,22]. In recent years, numerous designs for biomaterial alternatives have been realized[8,23]. These material

[1]Department of Energy, Environmental and Chemical Engineering, McKelvey School of Engineering, Washington University in St. Louis, St. Louis, MO, USA. [2]Carbon Utilization Redesign for Biomanufacturing (CURB) Engineering Research Center, St. Louis, MO, USA. [3]Synthetic and Systems Biology Innovation Hub and Department of Plant Pathology and Microbiology, Texas A&M University, College Station, TX, USA. [4]Department of Chemical and Biomedical Engineering, University of Missouri, Columbia, MO, USA. e-mail: joshua.yuan@wustl.edu

syntheses often utilize blending approaches to create biopolymeric composites comprised of polylactic acid (PLA), polyhydroxyalkanoate (PHA) such as polyhydroxybutyrate (PHB), starch, or cellulose[22,24]. However, these materials are limited in their mechanical performance or water resistance and thus have challenges in industrial adoption[25]. Additionally, the bioplastics that have the best mechanical properties, are the hardest to biodegrade[26]. For example, PLA has a high tensile strength around 65 MPa but is recalcitrant to biodegradation in soil and marine environments, often requiring industrial composting conditions[22,27,28]. For this reason, PLA is considered compostable, instead of biodegradable[29]. Designing biodegradable PLA has been a well-sought goal for bioplastics advancement[23]. As compared to PLA, PHB films are more readily biodegradable, though PHB is much less mechanically robust than PLA[30–32]. Alternative synthetic strategies have emerged to enhance biodegradability, such as electrospinning. However, these materials demonstrate a significant decrease in mechanical performance, and increased gas and liquid permeability[33]. Aside from mechanical strength and biodegradability, other highly sought-after features of plastic materials include: water stability, air impermeability, transparency, and printability. It is highly challenging to achieve broad multi-functionality in a single material to address all these needs. The LEAFF composite addresses these challenges through its layered film structure, which combines the individual advantages of CNF and PLA materials, while minimizing their disadvantages by leveraging the synergistic effects that emerge through the interfacial crosslinking of the two polymers. The LEAFF overcomes the previous paradigm of biomaterials engineering where a material can either be strong or biodegradable, achieving both robust mechanical performance and high biodegradability in ambient condition soil.

To create a biodegradable and mechanically robust plastic alternative, with the aforementioned important features, we turned to nature to look for a biomimetic material design. For centuries, cultures around the world have used plant leaves as a material for food in cooking, packaging, and storage[34]. The plant leaf is a complex composite material composed of an intricate network of water (xylem) and sugar (phloem) transport vasculature, photosynthetic cells, and a strong internal structure from cellulose-rich cell walls, all covered by a thin wax-like coating called cutin[35]. Inspired by the use of natural materials for food packaging and the natural leaf's attributes, we reconstituted the material morphology of plant leaves using sustainable polymers. This resulted in engineering the biomimetic Layered, Ecological, Advanced, multi-Functional Film (LEAFF) comprised of a strong core cellulose nanofiber (CNF) structure, a polylactic acid (PLA) coating, and a hexamethylene diisocyanate (HMDI) crosslinker to compatibilize their interface. HMDI is a safe cross-linker utilized in tissue engineering, drug delivery, and biomedical implant applications[36–42]. Additionally, all of these materials have individually been used in FDA-approved food packaging applications[38,43–46]. Leveraging this crosslinking approach, we coated CNF films in PLA to synergistically leverage the mechanical strength of CNF films and the gas barrier properties and water stability of PLA[27,47–49]. The resulting film exhibits greater tensile strength and modulus than biopolymeric materials, and even surpasses those of polyethylene and polypropylene, the most used petrochemical materials[22]. Furthermore, this mechanical advantage comes at no cost to biodegradation, instead driving PLA to completely biodegrade in soil at ambient conditions. Furthermore, the LEAFF design also achieves multifunctionality including water stability, gas impermeability, and others. The multilayer film design of LEAFF represents a broadly applicable strategy to manufacture mechanically robust and rapidly biodegradable films utilizing synergistic multi-functionality. Thus, the biomimetic LEAFF represents a new paradigm of sustainably derived, engineered bioplastics.

Results

The bioinspired design of the LEAFF

Evolved over millions of years to sustain photosynthesis and biological life cycle reproduction, the natural plant leaf is structured to: provide large surface area to receive light and split water; control barrier properties to transport CO_2 into leaf structure, remove O_2 and H_2O from the plant organelle; and degrade within the seasonal life cycle timeframe[35,50]. All these attributes, including water barrier and biodegradability, are highly desirable properties for plastics films. From materials perspective, these features are enabled by a multilayer film design comprised of a porous core layer of plant cells and cellulose fibers coated in a wax-like material called cutin[35].

However, natural leaves have limitations in their ability to package food due to low material properties, with a tensile strength between 1-6 MPa and low transparency[51]. We have improved upon these limitations in a new biomimetic material – the LEAFF. To coat a PLA layer on a core CNF film, dip-coating was chosen as it a common technique in food packaging material synthesis and allows for uniform layer deposition[52–54]. The coating parameters were optimized experimentally (Note S1). The as-prepared films ranged from 20-40 µm, in the expected range for their real application. Additionally, LEAFFs are comprised of 98% CNF, 2% PLA, and 0.02% HMDI by mass (Fig. S6). The choice of PLA as a coating material was made to ensure high mechanical performance, high film transparency, water resistance, and decent vapor barrier transport properties. As summarized in Fig. 1, the LEAFF was designed not only to have the properties relevant to food packaging applications but to be rapidly biodegradable (Fig. 1).

LEAFF's multilayer morphological characterization

First, the morphology of the film was characterized to validate that the designed material architecture was actualized (Fig. 2A). Through Fourier transform infrared (FTIR) spectroscopy, the PLA coating on the surface of the CNF film is observed as a new absorbance peak at 1760 cm^{-1}, which corresponds to the ester group carbonyl of the PLA polymer. Additionally, after crosslinking there is a slight increase in the absorbance of the carbamate associated peaks between 1640–1680 cm^{-1}, signaling the appearance of the carbamate functional group from successful HMDI crosslinking (Fig. 2B). To verify that the PLA coating is covering the surface of the composite films, contact angle analysis was conducted (Fig. 2C, D). Neat CNF films present a contact angle of 48.8° ± 3.3°, as expected for a hydrophilic material and in agreement with literature for these materials[55]. Contact angles of both the PLA-coated CNF film and the crosslinked PLA-coated CNF film were comparable to that of the neat and crosslinked PLA films. At an average of 71.9° ± 3.0, the LEAFF's contact angles closely agree with that of neat PLA obtained experimentally and from literature[37]. The addition of the crosslinker does not further increase the contact angle.

To understand the thermal properties of the LEAFF, differential scanning calorimetry (DSC) and thermogravimetric (TGA) analyses were carried out (Fig. 2E–G). From the DSC thermograms, the glass transition temperature for all of the films falls in a similar range, around 58 °C, in agreement with literature for the T_g of PLA[56]. There is a marked decrease in the cold crystallization temperature (T_{cc}) due to crosslinking from 115 °C to 111 °C for the CNF/PLA and LEAFF, respectively (Fig. 2E). The same trend is observed for the neat PLA and crosslinked PLA films. Interestingly, this decrease in the T_{cc} is concomitant with a decrease in overall PLA crystallinity in both cases. There are two observed melt peaks in the CNF/PLA composites, T_{m1} between 147.8 °C and 149.0 °C and T_{m2} between 154.9 °C and 155.3 °C (Figs. S1–2). The more thermodynamically stable crystal structure is due to the α-crystal structure and the less stable structure is the result of the α′-crystal[57]. In the crosslinked LEAFF, there is a significant increase in the more thermodynamically stable α-crystal content seen in the increased melt enthalpy contributing to the appearance of a

https://doi.org/10.1038/s41467-025-61693-2

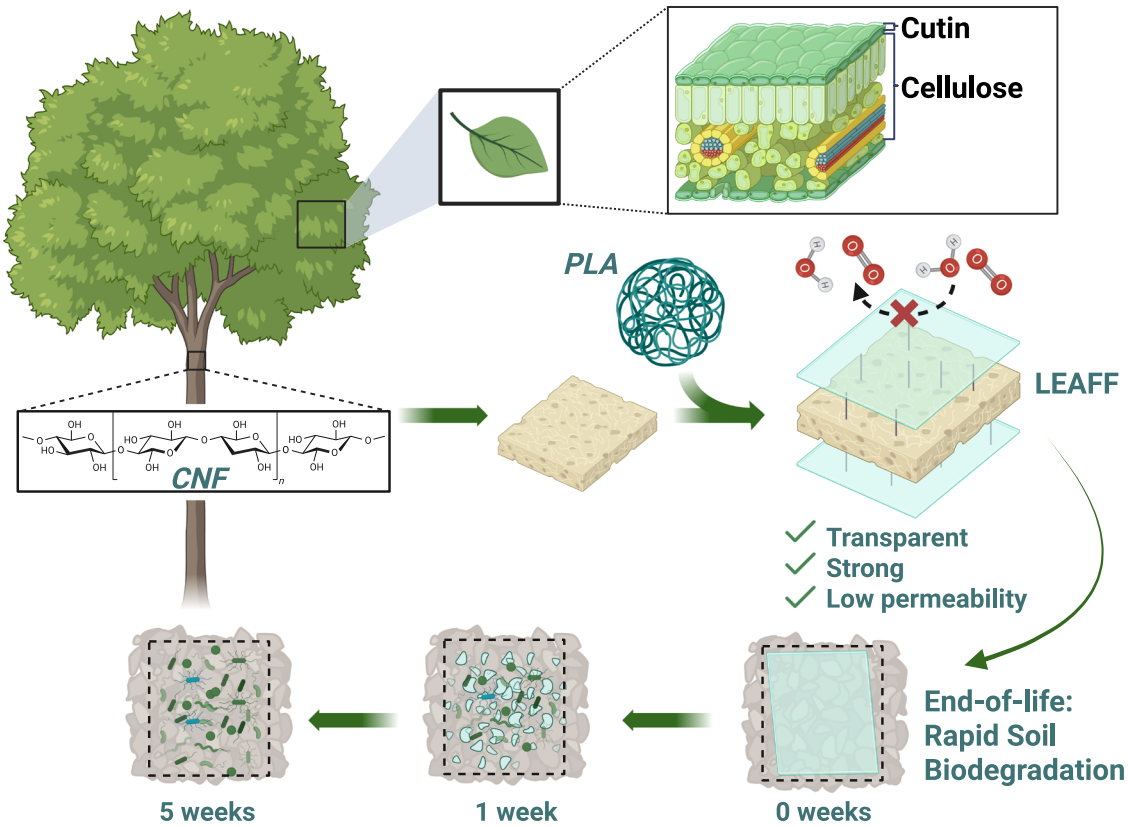

Fig. 1 | Representation of LEAFF life cycle. Depicted is the synthetic route of LEAFF synthesis from sustainably derived cellulose fibers coated with the biopolymer polylactic acid. The LEAFF film shows exceptional barrier properties to oxygen and water along with high transparency and a high tensile strength. At the end of its life, LEAFF can rapidly biodegrade due to microbial digestion in less than 5 weeks. Created in BioRender. Dhatt, P. (https://BioRender.com/gvyekxr).

second melt peak at 155 °C on the CNF/PLA composites' thermograms[58]. The same trend is observed in the neat PLA and crosslinked PLA samples (Fig. 2E). The presence of the CNF allows a location for preferable PLA crystallization into the α-crystalline structure, representing 23.2% of the total PLA crystal structures (Table 1). Furthermore, the presence of the crosslinker compatibilizes the CNF and PLA interface, increasing the α-crystal content to 45.2% (Table 1). Thus, the crosslinked LEAFF has more crystal content of the more thermodynamically stable α-crystal than the un-crosslinked CNF/PLA film. The TGA and derivative thermogravimetric (DTG) curves reveal a similar thermal degradation profile for all the CNF based films, with an increase in the temperature of maximum degradation rate from 337.1 °C to 338.9 °C with the PLA coating, and a further increase to 339.3 °C following crosslinking (Fig. 2F, G; Table 2). X-ray diffraction (XRD) was conducted on the composite films to understand the effect of PLA coating and crosslinking on the crystallinity of CNF and PLA composites (Fig. 2H). The XRD reveals a decrease in CNF crystallinity index (CI) of the CNF film from 76.5% to 74.6% due to PLA coating, but an increase to 82.0% due to crosslinking-driven densification of the film.

Finally, scanning electron microscopy (SEM) was used to visualize the morphology of the LEAFF. The natural plant leaf's core fibrous structure was recapitulated as fibrous bundles, seen in the LEAFF's core CNF layer (Figs. 2I, S3–4). Additionally, the PLA coating is visible as a separate layer coating the CNF film (Fig. 2J). The LEAFF also showed the least prevalence of holes on the film surface compared to the non-crosslinked CNF/PLA and neat PLA films (Fig. S5). SEM was also used to estimate the film thickness, which ranged from 20-40 μm, with a PLA coating thickness ranging from 100-200 nm (Fig. S6). Together, these data showcase the successful coating of the CNF film and achievement of the architecture of the material design of the LEAFF.

The LEAFF shows stable mechanical performance in wet and dry conditions

The key property of food packaging material is tensile strength. In the LEAFF, the synergistic interplay and crystal contents of the crosslinked CNF and PLA composite are realized in its robust mechanical performance. The tensile strength of the LEAFF composite is 118.1 ± 8.6 MPa, far surpassing those of any of its constituent materials (Fig. 3A, D; and Table 3). The elastic modulus (or Young's modulus) of the LEAFF is 10.6 ± 1.2 GPa, notably higher than CNF or PLA composite films (Fig. 3A, F; and Table 3). The tensile strength and modulus of the LEAFF surpass those of the conventional petrochemical packaging plastics used today (Table S1)[22,59].

In addition to general material properties, the LEAFF was also characterized for applications specific to food packaging. One such application is that of water resistance for storage of moist foodstuffs. The LEAFF meets this criterion as its mechanical properties show great resistance to water after 36 h water submersion (Fig. 3B–G). Up to 14 d of water submersion performance was tested for LEAFF films with no further decrease in tensile strength (Fig. S7). LEAFF's increased water stability is also observed in its decreased swelling due to 24 h water submersion, which approaches that of neat PLA (Fig. 3C). The LEAFF retains a tensile strength of 91.1 ± 6.9 MPa under these conditions, representing 77% of its dry mechanical strength. Neat CNF and CNF/PLA films degrade more significantly in their tensile strength, showing 51% and 68% retention, respectively (Fig. 3D–G). This phenomenon is due to the surface morphology of the LEAFFs compared to the CNF/PLA films. SEM imaging reveals that the CNF/PLA films have holes on their surface which can facilitate water to transport through the more hydrophobic PLA coating and dissolving the core CNF layer (Fig. S5). The neat PLA films show

https://doi.org/10.1038/s41467-025-61693-2

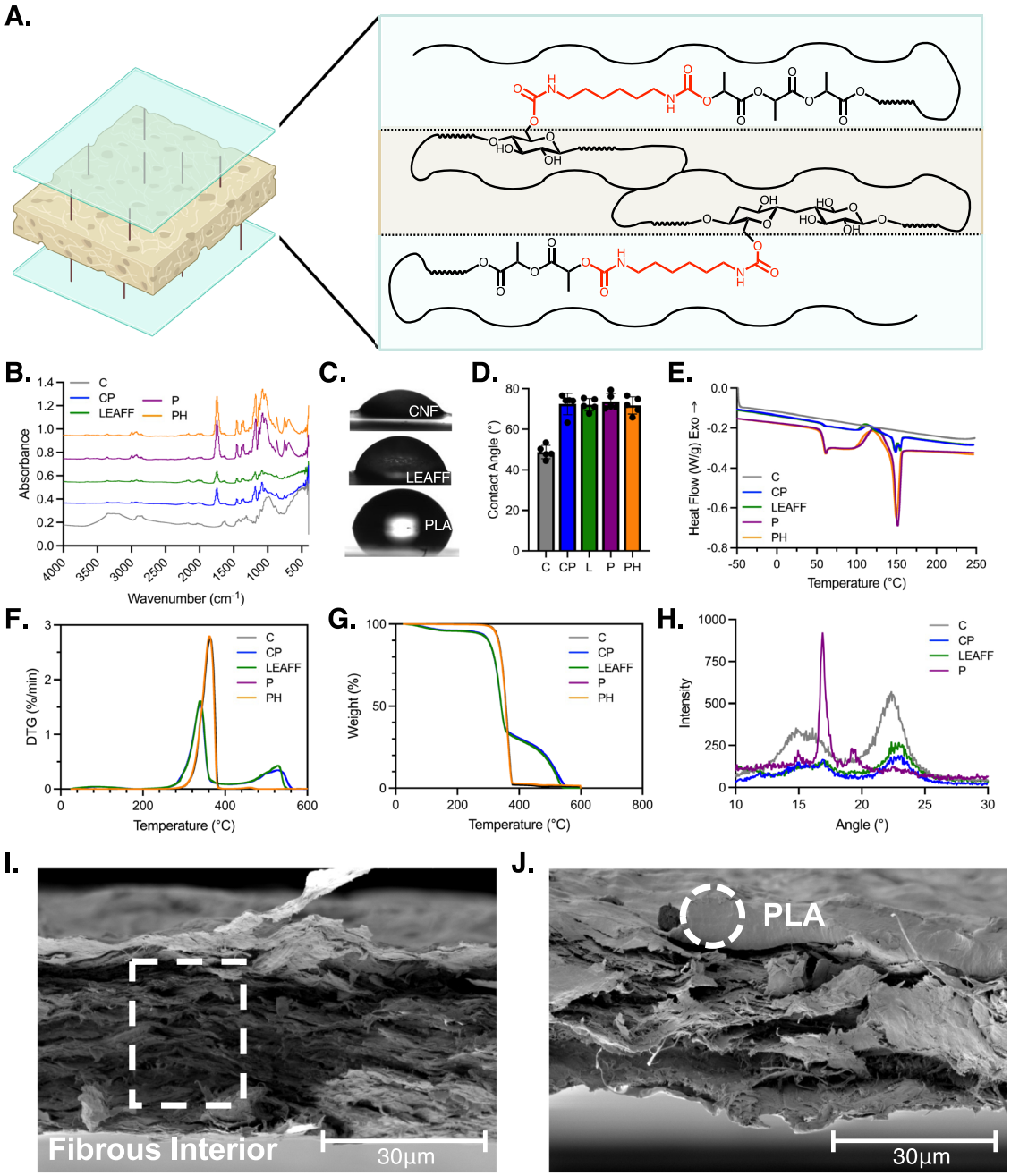

Fig. 2 | LEAFF Film Design and Characterization. A The LEAFF composite film consists of a porous CNF core (white) coated in PLA (light blue). The HMDI cross-linker (brown) is then cured to allow for interfacial bonding between the CNF and PLA layers. Created in BioRender. Dhatt, P. (https://BioRender.com/411y44v). **B** Fourier transform infrared spectra of composite and control films. **C** Contact angle 1 µL water droplet images on film surface. **D** Water contact angle results for control and composite films, N = 5. Individual data points are shown as black dots. **E** Differential scanning calorimetry second heating thermograms for composite films. Exothermy read as positive values. **H** X-ray diffractometry curves for composite films. **F** Thermogravimetric analysis in weight change (%) for composite films. **G** Derivative thermogravimetric analysis in weight change per min (%/min) for composite films. **H** XRD curves for composite and control films. **I** ESEM imaging of CNF control film cross-section. **J** ESEM image of LEAFF composite cross-section. Films: Neat CNF (C, gray), CNF/PLA (CP, blue), LEAFF (L, green), neat PLA (P, purple), PLA/HMDI (PH, orange). Data: mean ± SEM.

higher strength retention percentage, but at only 65.0 ± 1.8 MPa, the wet LEAFF are similar to or stronger than all other films tested in any condition (Fig. 3D). The elastic moduli of the composite films display a similar trend. The wet LEAFF has an elastic modulus of 6.7 ± 0.7 GPa, which is a similar or greater modulus than all samples' dry performance (Fig. 3F). Thus, together with the hydrophobicity measurement by contact angle (Fig. 2C, D) our results suggest that LEAFF would have broad applicability for wet and dry packaging applications, though is not applicable for oil-type applications. LEAFF applications could include moisture sensitive products and products with humid contents.

Multifunctionality of the LEAFF

Along with its mechanical performance, food packaging materials demand high oxygen and water vapor transmission resistance and high transparency[8]. Compared to petrochemical plastics, the LEAFF has high resistance to oxygen and water transmission (Fig. 4A, and Table S1). Through ASTM E96 testing of our films at 95% humidity and

Table 1 | Composite film crystal content analysis

Sample	T_g (°C)	T_{m1} (°C)	T_{m2} (°C)	ΔH_m (J/g)	$\chi_{PLA,\alpha}$
CNF					
CNF/PLA	58.5	149.0	155.3	1.8	23.2%
LEAFF	57.6	147.8	154.9	1.5	45.2%
PLA	59.0	151.6		24.2	
PLA/HMDI	57.8	149.8		22.9	

The results for CNF crystallinity are calculated from XRD curves while the PLA crystallinity results are calculated from DSC thermograms. T_g glass transition temperature, T_{cc} cold crystallization temperature, ΔH_{cc} enthalpy of cold crystallization, T_{mi} melting temperature of peak of i, ΔH_m enthalpy of melting, $\chi_{PLA,\alpha}$ crystal content of the α cystalline structure in PLA.

Table 2 | Thermogravimetric analysis results

Sample	$T_{5\%}$	$T_{50\%}$	$T_{95\%}$	T_{mdr}	Residue (%)
CNF	243.7	341.8	535.1	337.1	0.013
CNF/PLA	263.0	342.3	536.2	338.9	0.377
LEAFF	251.3	342.1	527.4	339.3	0.001
PLA	323.7	357.3	375.4	363.5	0.971
PLA/HMDI	323.1	356.7	375.0	361.9	1.545

$T_{X\%}$ Temperature at X% degradation, T_{mdr} temperature at the maximum rate of degradation, Residue – weight percentage at 600 °C.

25 °C, it is shown that the LEAFF water vapor permeability (WVP) is 0.794 g mm m^{-2} d^{-1} which is significantly lower than the neat CNF, neat PLA, and un-crosslinked CNF/PLA films which are 1.146, 1.162, 1.382 g mm m^{-2} d^{-1}, respectively. For oxygen barrier evaluation, the oxygen transmission rates (OTR) and oxygen permeance (OP) of the films were characterized (Fig. 4A–C). Due to the densification of the film after crosslinking, LEAFFs have an OTR of 0.772 cm^3 m^{-2} day^{-1} atm^{-1} and OP 1.37 cm^3 mm m^{-2} day^{-1} atm^{-1}. The neat PLA films show the most permeability to oxygen with an average OTR of 108.5 cm^3 m^{-2} day^{-1} atm^{-1} and OP of 630.31 cm^3 mm m^{-2} day^{-1} atm^{-1}, agreeing with literature for neat PLA films[8]. The neat CNF and CNF/PLA composite films show similar OTR averages of 1.8 and 1.97 cm^3 m^{-2} day^{-1} atm^{-1}, respectively. The oxygen permeability of the CNF/PLA composite film is slightly elevated from the neat CNF film due to the immiscibility of the two polymers leading to structural defects at their interface, allowing for more oxygen to transfer through the film. In terms of oxygen transmission, LEAFF films present a much higher barrier to oxygen than the commonly used neat polyolefin-based packaging films. Additionally, the water vapor barrier of LEAFF films are above olefin-derived plastics, in the range of other biopolymeric materials. Overall, the gas barrier properties position LEAFF films well for applications in packaging due to comparable gas barrier properties with commercially relevant polymer films such as polyethylene, polypropylene, and polystyrene (Table S1).

The LEAFF also exhibits high transparency with a percent transmittance of approximately 49% compared to 33% and 29% for CNF and CNF/PLA films, respectively (Figs. 4D, S8). This increase in film transparency was engineered by controlling for three physical properties of the film. The first two factors are both caused by the chemical crosslinking used in this system which compatibilizes the CNF/PLA interface and changes the PLA crystal structure. Additionally, PLA and CNF have very similar indices of refraction allowing for minimal light scattering[60–62]. The similarity in the transparency of the LEAFF compared to neat PLA films was observed as text is entirely legible through both films (Fig. 4E). LEAFF shows similar performance to the neat PLA film for readability. Finally, the printability of the LEAFFs was compared with conventional A4 printing paper and imaged at various resolutions to understand the printing fidelity of the film material at the consumer level. The LEAFF showcases surface printability showing less smearing or drifting of ink when compared to conventional printing paper (Fig. 4F).

Biodegradation

One of the major limitations of PLA use as a commodity bioplastic is that it is not soil biodegradable. PLA degradation has to be achieved through composting at an elevated temperature[27,28]. This substantially complicates its end-of-life (EOL) treatment. There is increasing attention on the end-of-life (EOL) impact for new materials that are used in high-quantity applications such as packaging materials[4]. This focus comes as bans are increasingly placed on plastic products due to their negative environmental impacts[18]. One recent study achieved PLA biodegradability through enzyme compositing, though the cost of enzyme production remains high[23]. LEAFF was designed to be entirely soil biodegradable through much simpler design and yet achieves both stronger mechanical properties and multi-functionality.

The biodegradability of LEAFF was investigated in soil under ambient conditions to mimic the true EOL conditions for the end-user of this material. The LEAFF is confirmed to have no significant toxicity on microbial growth and a reduced degree of microbial surface adhesion than control CNF film (Fig. S9). The biodegradation results show that neat CNF films completely biodegrade in 5 weeks under ambient condition temperature (25 °C) and humidity (40-60% RH). However, surprisingly both the CNF/PLA films and LEAFF also show a large degree of degradation in 5 weeks while control neat PLA films show no sign of biodegradation under ambient conditions (Figs. 5A–C; and S10–15). The biodegradative performance was also measured under high humidity conditions, to model humidity during the summer, which resulted in LEAFF complete biodegradation in 3 weeks (Figs. S16–19). This result showcases the incredible advantage of LEAFF over both the conventional petrochemical plastics, which degrade on the order of hundreds to thousands of years, and the current bioplastic alternatives, which degrade on the order of years to decades[22,63]. The surfaces of the degrading films were imaged after 2 weeks and there is clear colonization in the cases of the CNF, CNF/PLA, and LEAFF but none for the PLA film (Fig. 5D, E).

To better understand the microbial community that is fostered in the LEAFF biodegradation microenvironment, whole genome sequencing (WGS) was conducted in a shotgun metagenomics approach with species-level identification. Notably, the microbial community that develops during LEAFF degradation is markedly different from that of the native soil. The LEAFF film fosters a more microbially diverse microenvironment (Figs. 5F, and S20; Table S2). This result is encapsulated in the Shannon, an alpha diversity index that includes both richness (species diversity) and evenness (uniformity of species prevalence). Larger Shannon values are associated with greater species diversity. The Shannon values for soil and LEAFF are 6.5 and 7.1, respectively. This increase in diversity is driven by an increase in the evenness of the microbial population, as the Pielou evenness index is greater for LEAFF than soil with no notable difference in Simpson's diversity (Table S2). This increase in microbial diversity likely helps facilitate LEAFFs biodegradation. Though, mostly the same set of genera and species are dominant in both conditions. One difference in species composition of note is the enhanced prevalence of the organism *Planctoellipticum variicoloris* in the LEAFF condition compared to the control. This organism is a Planctomycete and has recently been isolated from waste-water samples[64]. Interestingly, members of the *Planctomycetaceae*, such as *Planctopirus limnophila*, have been shown to have the rare ability for endocytosis-like macromolecular import[65]. We hypothesize that the emergence of the prevalence of this species due in the LEAFF biodegradation microenvironment may be due to this macromolecular import that could facilitate biopolymer degradation.

Our hypothesis is that the challenge of ambient condition PLA biodegradation is two-fold: one is a chemical limitation of energy

https://doi.org/10.1038/s41467-025-61693-2

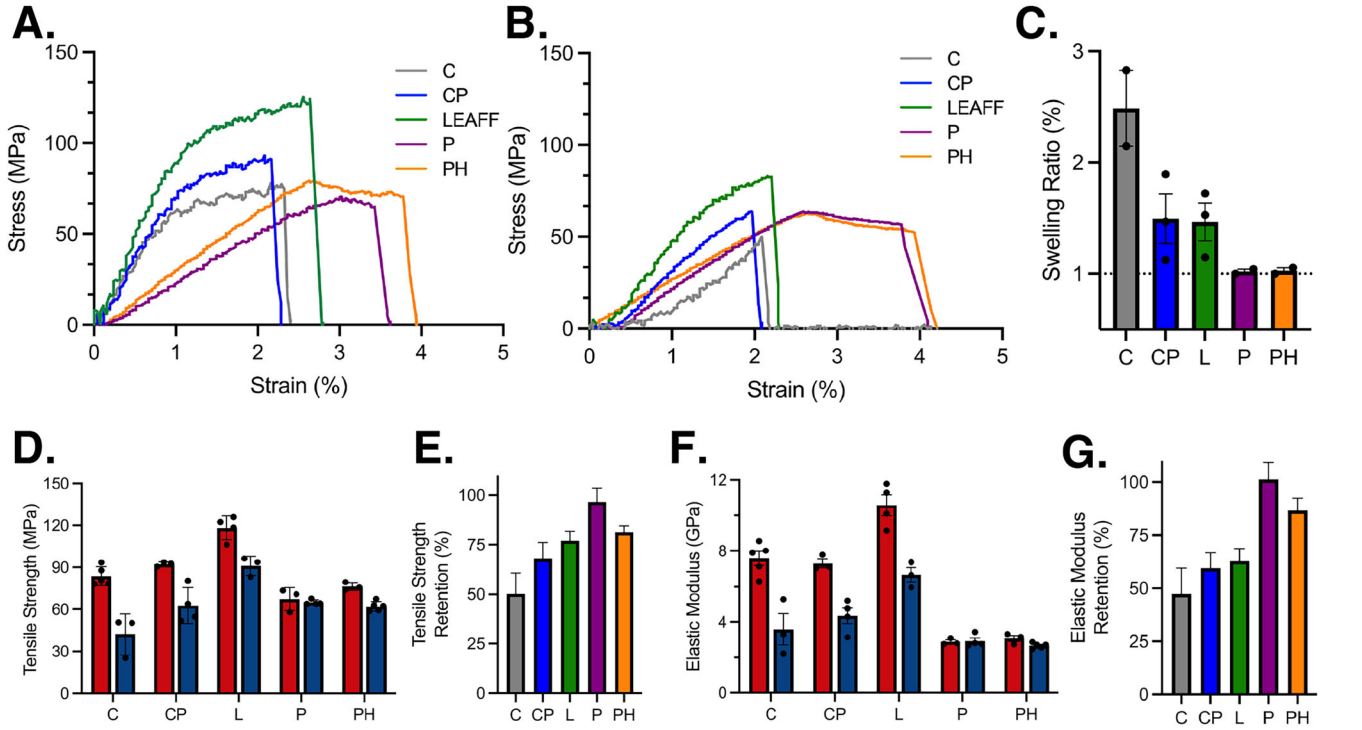

Fig. 3 | Mechanical properties of LEAFF films in wet and dry conditions. Monotonic stress-strain curves for (**A**) dry film and (**B**) wet films after 36 h water submersion. **C** Swelling ratio of composite films after 24-36 h water submersion, $N = 2$. **D** Comparison tensile strength elastic modulus of dry (red) and wet (blue) composite films after 36 h water submersion, $N \geq 3$. **E** Retention % of tensile modulus (wet/dry) after 36 h water submersion, $N = 3$. **F** Comparison of dry (red) and wet (blue) elastic modulus (GPa), N ≥ 3. **G** Retention % of elastic modulus (wet/dry), $N = 3$. Films: Neat CNF (C, gray), CNF/PLA (CP, blue), LEAFF (L, green), neat PLA (P, purple), crosslinked PLA/HMDI (PH, orange). Individual data points are shown as black dots. Data: mean ± SEM.

Table 3 | Mechanical Properties of Composite Films

Sample	*E (GPa)*	*σ (MPa)*	*ε (%)*
CNF	7.6 ± 0.9	83.7 ± 6.7	2.1 ± 0.2
CNF/PLA	7.3 ± 0.4	92.2 ± 1.6	1.8 ± 0.3
PLA	2.9 ± 0.2	67.4 ± 8.3	2.8 ± 0.6
PLA/HMDI	3.1 ± 0.3	76.3 ± 2.9	3.7 ± 0.4
LEAFF	**10.6 ± 1.2**	**118.1 ± 8.6**	**2.1 ± 0.6**

E Elastic modulus, *σ* Ultimate tensile strength, *ε* Elongation at break. Data: mean ± s.d.

balance, and the other is a physical limitation imposed by the crystal structure of PLA. The breakdown of PLA consists of an initial energy input of ester bond hydrolysis followed by the released low-energy lactide monomer conversion to pyruvate before being shunted into central metabolism. Thus, we hypothesized that with the colocalization of high energy content cellulose fuels this energy deficient microbial metabolic process to increase PLA degradation. This is confirmed by the proliferation of the soil microbiome onto the LEAFF films but not neat PLA films. Additionally, we engineered the film to allow for cells and excreted hydrolytic enzymes to better access PLA polymer chains. Furthermore, the fibrous internal structure of CNF allows the soil microbes to grow and concentrate near the PLA material, further enhancing its biodegradation over that of neat PLA.

Discussion

The biomimetic LEAFF exhibits multifunctional performance in terms of its vapor barrier properties, mechanical strength, and transparency. PLA is the most widely used biopolymer, with significant avenues to scale-up, but it's main challenge of a lack of ambient condition biodegradability remained. LEAFFs overcome these challenges through engineering of PLA crystallinity. This microstructural design informs broadly of the methods to overcome the challenges of PLA and achieve high performance multifunctional materials that can still be biodegradable at ambient conditions.

However, some challenges remain to be addressed. For industrial adoption as a packaging material, LEAFF production needs to be scaled up. The industry already employs large-scale multilayer film extruders and laminators that could be used to scale up LEAFF production, though more work is still needed to understand how to recapitulate the structure of LEAFF. One additional benefit of scale up is this lamination can be done solvent-free, as PLA is a common thermoplastic for extrusion-based applications, especially in 3D printing. This would eliminate the usage of chlorinated solvents in PLA solvation.

Another of the remaining challenges in the field of bioplastics is the costs of raw materials[66]. Recent technological innovations in bioprocessing can produce CNF around $2,000/tonne[66,67]. Additionally, PLA is estimated to be produced at scale at $1,000-2,000/tonne[68]. These prices are now beginning to approach those of virgin polyethylene and polypropylene ($800-2,400/tonne)[69,70]. Taking into account that oil production is often governmentally subsidized, the costs trend yet closer toward parity[22]. Therefore, the LEAFF presents a multifunctional packaging film that can be a true sustainable replacement for a broad range of petrochemical plastic packaging materials while surpassing their mechanical performance and overcoming inherent challenges of biodegradability.

Method

Materials

Cellulose nanofibrils (CNF-slurry-SMC, prepared by supermass colloider, 20% wt) were purchased from Cellulose Lab (NB, Canada). Polylactic acid (PLA; GF45989881) with a 3–5 mm nominal granule size and average molecular weight (M_w) 193.3 kDa, Hexamethylene

https://doi.org/10.1038/s41467-025-61693-2

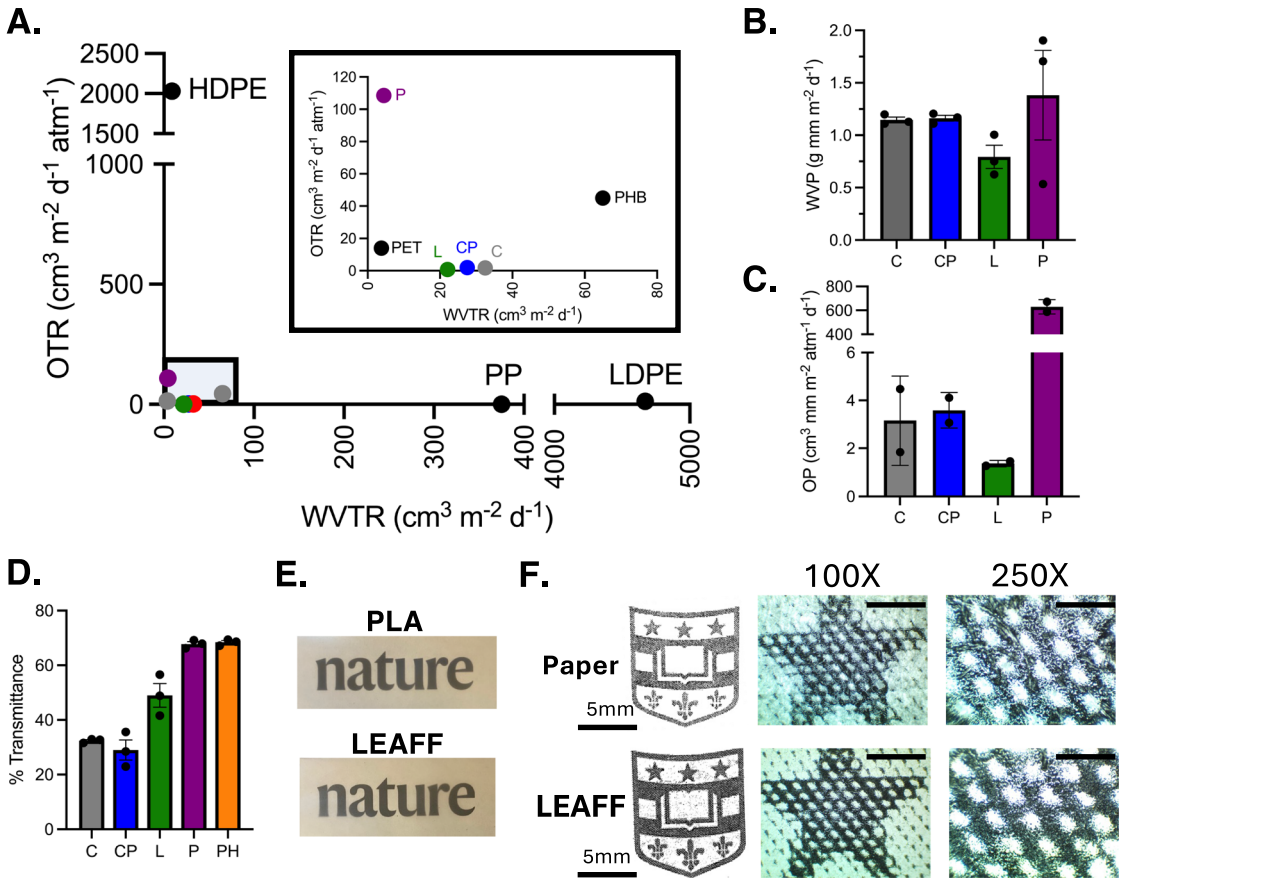

Fig. 4 | Evaluation of LEAFF films food packaging-specific properties. **A** Comparison of conventional petrochemical plastic oxygen and water vapor transmission rates compared to composite films. **B** Oxygen permeability (OP) analysis of composite films, N = 2. **C** Water vapor permeability analysis of composite films, N = 2. **D** Transparency (%Transmittance) of light through composite films at 600 nm, N = 3. **E** Readability of text through films, N = 2. **F** Printability assay conducted on conventional A4 printer paper and LEAFF films. Films are imaged under a microscope at 100X and 250X magnifications, N = 2. Films: High density polyethylene (HDPE), Low density polyethylene (LDPE), polypropylene (PP), Polyethylene terephthalate (PET), Polyhydroxybutyrate (PHB), Neat CNF (C, gray), CNF/PLA (CP, blue), LEAFF (L, green), neat PLA (P, purple), PLA/HMDI (PH, orange). Individual data points are shown as black dots. Data: mean ± SEM.

diisocyanate (HMDI; 8.22066, purity: > 99.0%), and dichloromethane (DCM; 650463-4 L, purity: > 99.9%) were purchased from Sigma-Aldrich (Saint Louis, MO). All materials were used as received without any further chemical modification. Ultrapure water was filtered by a Synergy® UV Water Purification System (EMD Millipore).

Preparation of films

Neat CNF films were prepared by preparing a 0.75% (w/v) CNF suspension in ultrapure water. Then, 30 mL of the suspension was cast into a petri dish and dried under ambient pressure, humidity, and at room temperature. Neat PLA films were prepared by pouring 25 mL of a pre-prepared 5% (w/v) solution of PLA in DCM into a 1 L borosilicate glass beaker, covering with a glass petri dish, and letting evaporate overnight. Composite films were synthesized from neat CNF films by dip coating the CNF films in 250 mL 5% PLA in DCM solution, with 0.8% (w_{HMDI}/w_{PLA}) HMDI crosslinker for CNF/PLA/HMDI films. Dip coating was conducted using a 40 mm/min speed with 5 s of full immersion of the film in the PLA coating solution and a 60 s drying time, for a total of 3 coatings. All films underwent the 80 °C thermal treatment for 4 h in an oven for crosslinking. Following thermal treatment, films were heat pressed at 50 °C for 30 min.

Material characterization

For all material characterizations, replicates represent distinct samples. Mechanical properties including ultimate tensile strength, Young's modulus, and elongation at break, were measured using a Mark-10 Tensile Tester with a 250 N load cell using IntelliMEASUR v2.3.3 software (Mark-10 Corp. Copiague, NY, USA). Samples were cut into Type V using a die and tested according to ASTM D638 with a traction speed of 25 mm min^{-1}. Sample thickness ranged from 20 - 40µm. All tests were conducted at room temperature under ambient pressure and humidity. Mechanical properties after water retention were tested under the same conditions after 36 h submersion of the films in DI water.

Contact angle was analyzed using an OCA 15EC contact angle goniometer equipped with 6.5X zoom lens using dpiMAX v2.4.142 software (DataPhysics, Charlotte, NC). A water droplet size of 1 µL was placed onto the film surface and once the droplet has reached its equilibrium position, it was imaged. The contact angle was calculated using OCA software.

Fourier transform infrared spectroscopy (FTIR) was conducted on composite film samples using a Thermo Scientific Nicolet iS20 (Waltham, MA). Spectra were recorded for the range of 4000–400 cm^{-1}.

An HP color LaserJet Pro M545Dn was used to print onto films for surface printability analysis. Films were prepared by cutting them into 3cm-by-3cm squares and taping the excess film on to a standard printer paper. Then, a standardized complex image (the Washington University in St. Louis logo) was printed onto this square and imaged under a Swift SW380t optical microscope using Swift imaging 3.0 software.

https://doi.org/10.1038/s41467-025-61693-2

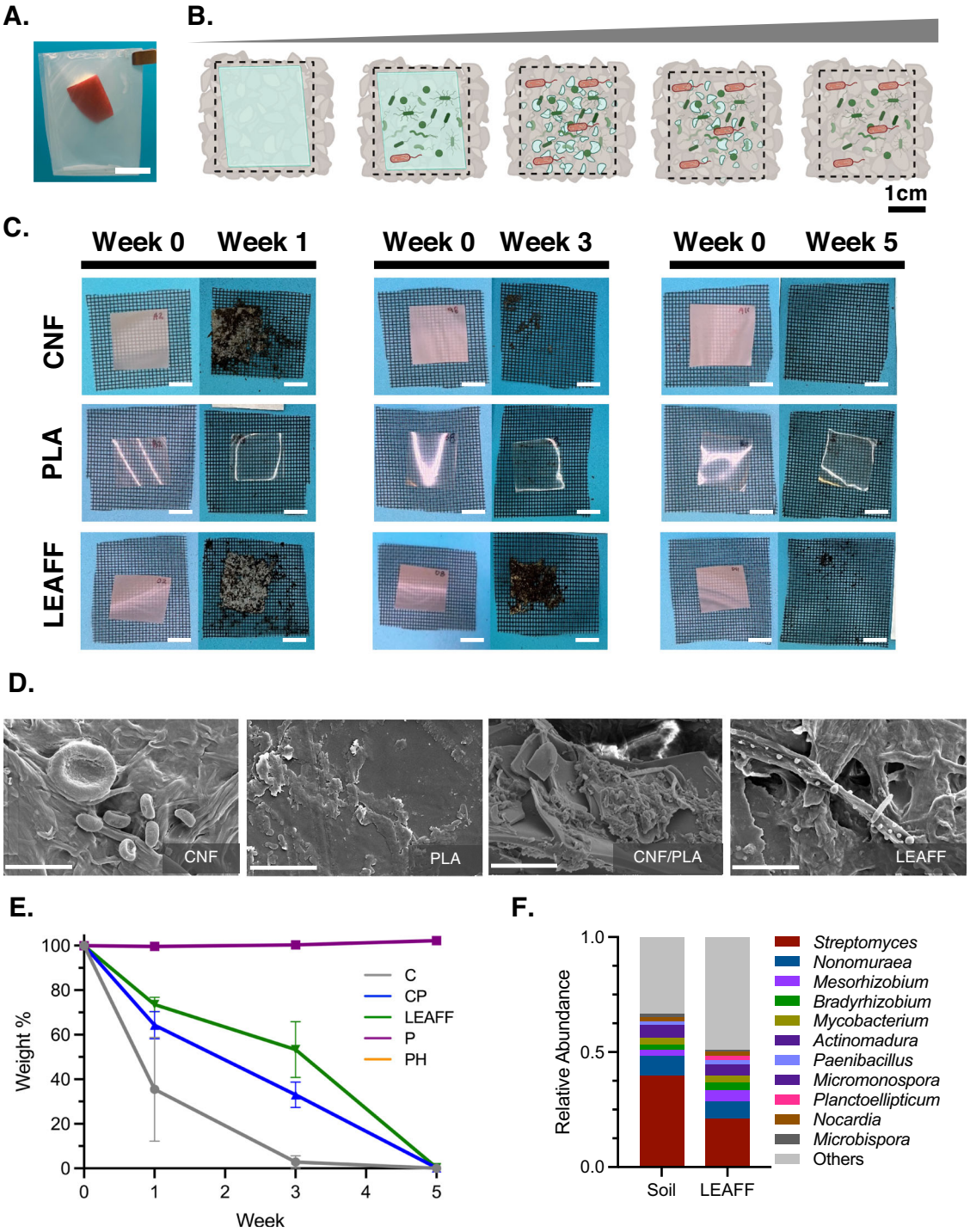

Fig. 5 | Rapid biodegradation of LEAFF films in soil. A Image of LEAFF film packaging application of an apple slice. Scale bar: 1 cm. **B** Representation of biodegradation of bioplastic films. Scale bar: 1 cm; bacteria not to scale. Created in BioRender. Dhatt, P. (https://BioRender.com/gu7gqlt). **C** Soil biodegradation photos for timepoints weeks 1, 3, and 5, showing their respective week 0 control. The biodegradation of control CNF and PLA are compared to the LEAFF. Scale bars: 1 cm. **D** SEM images of the degrading films at 2 weeks. Scale bar: 10μm. **E** Weight percentage remaining of composite films over the course of biodegradation. Films: Neat CNF (C, gray), CNF/PLA (CP, blue), LEAFF (L, green), neat PLA (P, purple), N = 3. Data: mean ± SEM. **F** Top 10 genera of microbial community by relative abundance.

A Tecan Infinite M200 Nano Plus plate reader with Tecan i-Control v3.9.1.0 software was used to measure transparency. Samples for each film were cut to fill the bottom of a 96-well clear bottom polypropylene plate. Measurements were taken from 300 to 1000 nm with a 10 nm step size.

Thermogravimetric Analysis (TGA) was performed using TA Instruments Q5500 (TA Instruments) to evaluate thermal degradation of samples in the range of 30–600 °C at a rate of 10 °C min^{-1} under an air flow rate of 25 mL min^{-1}. Derivative Thermogravimetric (DTG) plots were collected using TA Universal Analysis 2000 Software.

Differential calorimetric analysis (DSC) of films was conducted by using a TA DSC 2500 system using TA Instruments Trios v5.1.1.46572 (TA Instruments, New Castle, DE). The samples were analyzed using a heat-cool-heat cycle where samples are heated from room temperature to 250 °C at a heating rate of 10 °C min^{-1}, cooled to −50 °C, then heated to 250 °C. The first heat cycle is used to analyze degree of PLA

crystallinity using Eq. (1):

$$\chi_{PLA} = \frac{\Delta H_m}{\Delta H_m^0 \times w_{PLA}} \quad (1)$$

Where χ_{PLA} is the degree of crystallinity of PLA, ΔH_m is the measured value of PLA melting enthalpy, calculated by integrating of the area of the appropriate melting peak(s), ΔH_m^0 is the melting heat of pure crystalline PLA (assumed to 93.6 J g^{-1})[71]. It is assumed that the melt peak is entirely due to PLA melting. Using the third cycle, crystal content was calculated by Eq. (2):

$$\chi_\alpha = \frac{\alpha}{\alpha + \alpha'} \quad (2)$$

Where α is the PLA α-crystal content, α' is the PLA α'-crystal content.

The surface and cross-sectional morphologies of composite films were analyzed using Environmental Scanning Electron Microscopy (Thermofisher Quattro S ESEM) with Thermo Scientific User Interface v15.2.2 software. The ESEM was operated in secondary electron mode with an accelerating voltage of 2 kV. Samples were sputter coated with a thin layer (6 nm) of gold before imaging using a High Vacuum Sputter Coater (Leica ACE600). Cross section samples were prepared by freeze-cracking after liquid nitrogen submersion for 10 min.

The X-ray diffraction (XRD) patterns of the CNF, PLA, CNF/PLA, and full LEAFF samples were analyzed by a DMaxB X-ray Diffractometer (Rigaku, Japan) using MDI Datascan 5 software. The instrument is equipped with a Cu-Kα radiation source (λ = 0.154 nm) with a 2θ range of 10-30° and the operation voltage and current were maintained at 35 kV and 30 mA respectively with a step size of 0.05, and a dwell time of 7 s. For PLA only and LEAFFs the dwell time was raised to 15 s. The CNF film crystallinity index (CI) was then calculated by Eq. (3)[72]:

$$CI = \frac{(I_{002} - I_{AM})}{I_{002}} \times 100 \quad (3)$$

Where I_{AM} is the minimum between the (002) and (101) crystalline peaks at 2θ = 22.3° and 2θ = 18.5° respectively, and I_{002} is the intensity of the (002) peak.

Water Vapor and oxygen transmission assay

Water Vapor Transmission Rate measurements were recorded following ASTM E96. Briefly, a 20 mL glass vial was filled with 10 mL of water and film samples were fixed to the top of the vial. Then, the glass vials were left in an environmentally sealed oven at 95% humidity and 25 °C. After 24 h, the vials were removed and the weight loss of the vials were measured using a balance precise to 0.0001 g (Sartorius; Göttingen, Germany). This result yields water vapor transmission rates (WVTR), which were then normalized by the film thickness to yield water vapor permeability (WVP).

For oxygen transmission rate (OTR), films were sent out for measurement following ASTM D3985 using an Illinois Instrument Model 8001 (Flex-Pack Engineering, OH, USA). Briefly, 25 cm^2 samples were cut from each film to be tested. The results were normalized by film thickness to yield oxygen permeability (OP) results.

Microbial growth and adhesion assays

To assess microbial toxicity, growth curves with and without the presence of 2 cm^2 LEAFF film presence were conducted using *Escherichia coli* BL21(DE3) (New England Biolabs, MA, USA). For growth experiments *E. coli* were seeded into 50 mL Luria-Bertani (LB) media in a 250 mL baffled flask using an initial seeding density of OD_{600} = 0.02 from overnight LB preculture. The growth curve was quantified by OD_{600} measurements taken every 30 min.

To assess microbial adhesion, *Pseudomonas putida* KT2440 (ATCC 47054) was cultured overnight in LB to a final OD_{600} of 3. Then, 1 cm^2 LEAFF film squares were cut and dipped into the culture media for 30 s. Films were air dried for 30 min and then sputter coated in 6 nm of gold before SEM imaging.

Soil biodegradation

All films are cut to 2.5cm-by-2.5 cm rectangles and placed onto a fiberglass mesh with a pore size <0.5 mm^2. The mesh is included to allow for the film to maintain its position in the soil for imaging, while retaining contact with the soil. Then, 65 g of FoxFarm Ocean Forest potting soil (CA, USA) is added to 7cm-by-7cm square plastic planting pots and the films are buried 2 cm below the soil surface. Samples are kept in a closed chamber at 25 °C, and either 40–60% or 60–80% relative humidity (%RH). Every other day, 8 mL of water is gently added to each sample. Each week, three distinct films were sampled without replacement and photographed to measure biodegradation. Soil was gently removed from the top of each pot, making sure to not damage or dislodge the film underneath. After two weeks, films were imaged by SEM.

Microbial community profiling

Following biodegradation, genomic DNA was extracted from soil samples for untreated and LEAFF biodegradation soil sampled using a DNeasy PowerSoil Pro Kit (Qiagen, USA), following manufacturer's protocols. Genomic DNA was then sent to Novogene (CA, USA), to perform whole genome sequencing (WGS) for microbial community identification with a depth of 1 Gbp. Taxonomic classification was conducted using the Kraken2 software.

Visualization and software analysis

All calculations were conducted in Microsoft Excel. All graphs were constructed in GraphPad Prism 10. Graphic schematics and representations were designed with BioRender. All figures are published with permission from BioRender.

Reporting summary

Further information on research design is available in the Nature Portfolio Reporting Summary linked to this article.

Data availability

All data used to generate main text and Supplementary Figs. is available upon request from the corresponding author. All data needed to evaluate the conclusions in the paper are presented the paper, the supplementary materials, or Source Data file. Shotgun metagenomics data was deposited to NCBI SRA under BioProject PRJNA1249046 at http://www.ncbi.nlm.nih.gov/bioproject/1249046. Source data are provided with this paper.

References

1. Geyer, R., Jambeck, J. R. & Law, K. L. Production, use, and fate of all plastics ever made. *Sci. Adv.* **3**, e1700782 (2017).
2. Jambeck, J. R. et al. Plastic waste inputs from land into the ocean. *Science* **347**, 768–771 (2015).
3. Zheng, J. & Suh, S. Strategies to reduce the global carbon footprint of plastics. *Nat. Clim. Change* **9**, 374–378 (2019).
4. Law, K. L. & Narayan, R. Reducing environmental plastic pollution by designing polymer materials for managed end-of-life. *Nat. Rev. Mater.* **7**, 104–116 (2022).
5. Chen, Y., Awasthi, A. K., Wei, F., Tan, Q. & Li, J. Single-use plastics: Production, usage, disposal, and adverse impacts. *Sci. Total Environ.* **752**, 141772 (2021).
6. OECD. *Global Plastics Outlook: Economic Drivers, Environmental Impacts and Policy Options*. (Organisation for Economic Co-operation and Development, Paris, 2022).

7. Lebreton, L. C. M. et al. River plastic emissions to the world's oceans. *Nat. Commun.* **8**, 15611 (2017).
8. Sangroniz, A. et al. Packaging materials with desired mechanical and barrier properties and full chemical recyclability. *Nat. Commun.* **10**, 3559 (2019).
9. Zhang, J., Wang, L. & Kannan, K. Microplastics in house dust from 12 countries and associated human exposure. *Environ. Int.* **134**, 105314 (2020).
10. Leslie, H. A. et al. Discovery and quantification of plastic particle pollution in human blood. *Environ. Int.* **163**, 107199 (2022).
11. Amato-Lourenço, L. F. et al. Presence of airborne microplastics in human lung tissue. *J. Hazard. Mater.* **416**, 126124 (2021).
12. Blackburn, K. & Green, D. The potential effects of microplastics on human health: What is known and what is unknown. *Ambio* **51**, 518–530 (2022).
13. Van der Laan, L. J. W., Bosker, T. & Peijnenburg, W. J. G. M. Deciphering potential implications of dietary microplastics for human health. *Nat. Rev. Gastroenterol. Hepatol.* **20**, 340–341 (2023).
14. Ghosh, S. et al. Microplastics as an emerging threat to the global environment and human health. *Sustainability* **15**, 10821 (2023).
15. Fleury, J.-B. & Baulin, V. A. Microplastics destabilize lipid membranes by mechanical stretching. *Proc. Natl. Acad. Sci.* **118**, e2104610118 (2021).
16. Ford, H. V. et al. The fundamental links between climate change and marine plastic pollution. *Sci. Total Environ.* **806**, 150392 (2022).
17. Andreoni, V., Saveyn, H. G. M. & Eder, P. Polyethylene recycling: waste policy scenario analysis for the EU-27. *J. Environ. Manag.* **158**, 103–110 (2015).
18. Jia, L., Evans, S. & Linden, S. van der. Motivating actions to mitigate plastic pollution. *Nat. Commun.* **10**, 4582 (2019).
19. Herberz, T., Barlow, C. Y. & Finkbeiner, M. Sustainability assessment of a single-use plastics ban. *Sustainability* **12**, 3746 (2020).
20. Single Use Packaging Market - Size, Share & Industry Report. https://www.mordorintelligence.com/industry-reports/single-use-plastic-packaging-market (2023).
21. Gross, R. A. & Kalra, B. Biodegradable polymers for the environment. *Science* **297**, 803–807 (2002).
22. Rosenboom, J.-G., Langer, R. & Traverso, G. Bioplastics for a circular economy. *Nat. Rev. Mater.* **7**, 117–137 (2022).
23. Guicherd, M. et al. An engineered enzyme embedded into PLA to make self-biodegradable plastic. *Nature* **631**, 884–890 (2024).
24. Surendren, A., Mohanty, A. K., Liu, Q. & Misra, M. A review of biodegradable thermoplastic starches, their blends and composites: recent developments and opportunities for single-use plastic packaging alternatives. *Green. Chem.* **24**, 8606–8636 (2022).
25. Grushkin, D. Breaking the mold. *Nat. Biotechnol.* **29**, 16–18 (2011).
26. Bergeson, A. R., Silvera, A. J. & Alper, H. S. Bottlenecks in biobased approaches to plastic degradation. *Nat. Commun.* **15**, 4715 (2024).
27. Slezak, R., Krzystek, L., Puchalski, M., Krucińska, I. & Sitarski, A. Degradation of bio-based film plastics in soil under natural conditions. *Sci. Total Environ.* **866**, 161401 (2023).
28. Royer, S.-J., Greco, F., Kogler, M. & Deheyn, D. D. Not so biodegradable: polylactic acid and cellulose/plastic blend textiles lack fast biodegradation in marine waters. *PLOS ONE* **18**, e0284681 (2023).
29. Narancic, T. et al. Biodegradable plastic blends create new possibilities for end-of-life management of plastics but they are not a panacea for plastic pollution. *Environ. Sci. Technol.* **52**, 10441–10452 (2018).
30. Luzier, W. D. Materials derived from biomass/biodegradable materials. *Proc. Natl. Acad. Sci.* **89**, 839–842 (1992).
31. Akdoğan, E. et al. Accelerating the environmental biodegradation of poly-3-hydroxybutyrate (PHB) via plasma surface treatment. *Bioresour. Technol. Rep.* **25**, 101719 (2024).
32. Wang, G., Huang, D., Ji, J., Völker, C. & Wurm, F. R. Seawater-degradable polymers—fighting the marine plastic pollution. *Adv. Sci.* **8**, 2001121 (2020).
33. Gasparyan, K. G., Tyubaeva, P. M., Varyan, I. A., Vetcher, A. A. & Popov, A. A. Assessing the biodegradability of PHB-based materials with different surface areas: a comparative study on soil exposure of films and electrospun materials. *Polymers* **15**, 2042 (2023).
34. Kora, A. J. Leaves as dining plates, food wraps and food packing material: importance of renewable resources in Indian culture. *Bull. Natl. Res. Cent.* **43**, 205 (2019).
35. Serbin, S. P. & Townsend, P. A. *Scaling Functional Traits from Leaves to Canopies*. in *Remote Sensing of Plant Biodiversity* (eds. Cavender-Bares, J., Gamon, J. A. & Townsend, P. A.) 43–82 (Springer International Publishing, Cham, 2020).
36. Jeong, J.-H. et al. Anti-Tumoral Effect of the Mitochondrial Target Domain of Noxa Delivered by an Engineered Salmonella Typhimurium. *PLoS ONE* **9**, e80050 (2014).
37. Parikh, B. H. et al. A bio-functional polymer that prevents retinal scarring through modulation of NRF2 signalling pathway. *Nat. Commun.* **13**, 2796 (2022).
38. Weems, A. C., Arno, M. C., Yu, W., Huckstepp, R. T. R. & Dove, A. P. 4D polycarbonates via stereolithography as scaffolds for soft tissue repair. *Nat. Commun.* **12**, 3771 (2021).
39. Xu, J. & Song, J. High performance shape memory polymer networks based on rigid nanoparticle cores. *Proc. Natl. Acad. Sci.* **107**, 7652–7657 (2010).
40. Ham, H. O. et al. In situ regeneration of bioactive coatings enabled by an evolved Staphylococcus aureus sortase A. *Nat. Commun.* **7**, 11140 (2016).
41. Chen, S. et al. Mechanically and biologically skin-like elastomers for bio-integrated electronics. *Nat. Commun.* **11**, 1107 (2020).
42. Choi, Y. S. et al. Stretchable, dynamic covalent polymers for soft, long-lived bioresorbable electronic stimulators designed to facilitate neuromuscular regeneration. *Nat. Commun.* **11**, 5990 (2020).
43. Boyer, J. C., Taylor, L. W. & Nylander-French, L. A. Viability of cultured human skin cells treated with 1,6-hexamethylene diisocyanate monomer and its oligomer isocyanurate in different culture media. *Sci. Rep.* **11**, 23804 (2021).
44. Inventory of Effective Food Contact Substance (FCS) Notifications. https://www.cfsanappsexternal.fda.gov/scripts/fdcc/?set=FCN&id=2263&sort=FCN_No&order=DESC&startrow=1&type=basic&search=polylactic%20acid (2022).
45. Inventory of Effective Food Contact Substance (FCS) Notifications. https://www.cfsanappsexternal.fda.gov/scripts/fdcc/?set=FCN&id=1887&sort=FCN_No&order=DESC&startrow=1&type=basic&search=cellulose%20 (2018).
46. Inventory of Effective Food Contact Substance (FCS) Notifications. https://www.cfsanappsexternal.fda.gov/scripts/fdcc/?set=FCN&id=1901&sort=FCN_No&order=DESC&startrow=1&type=basic&search=hexamethylene%20diisocyanate (2018).
47. Liu, Y. et al. A review of cellulose and its derivatives in biopolymer-based for food packaging application. *Trends Food Sci. Technol.* **112**, 532–546 (2021).
48. Carosio, F. et al. Efficient gas and water vapor barrier properties of thin poly(lactic acid) packaging films: functionalization with moisture resistant nafion and clay multilayers. *Chem. Mater.* **26**, 5459–5466 (2014).
49. Anggarini, U. et al. A highly water-selective carboxymethylated cellulose nanofiber (CNF-CMC) membrane for the separation of binary (water/N2) and ternary (water/alcohols/N2) systems in vapor-permeation. *J. Membr. Sci.* **691**, 122229 (2024).
50. Ustin, S. L. & Jacquemoud, S. How the Optical Properties of Leaves Modify the Absorption and Scattering of Energy and Enhance Leaf Functionality. in *Remote Sensing of Plant Biodiversity* (eds.

Cavender-Bares, J., Gamon, J. A. & Townsend, P. A.) 349–384 (Springer International Publishing, Cham, 2020).
51. Wang, S., Ren, L., Liu, Y., Han, Z. & Yang, Y. Mechanical characteristics of typical plant leaves. *J. Bionic Eng.* **7**, 294–300 (2010).
52. Ruzi, M., Celik, N. & Onses, M. S. Superhydrophobic coatings for food packaging applications: a review. *Food Packag. Shelf Life* **32**, 100823 (2022).
53. Rio, E. & Boulogne, F. Withdrawing a solid from a bath: How much liquid is coated?. *Adv. Colloid Interface Sci.* **247**, 100–114 (2017).
54. Puetz, J. & Aegerter, M. A. Dip Coating Technique. in *Sol-Gel Technologies for Glass Producers and Users* (eds. Aegerter, M. A. & Mennig, M.) 37–48 (Springer US, Boston, MA, 2004)..
55. Rbihi, S., Aboulouard, A., Laallam, L. & Jouaiti, A. Contact angle measurements of cellulose based thin film composites: wettability, surface free energy and surface hardness. *Surf. Interfaces* **21**, 100708 (2020).
56. Strutynski, C. et al. 4D Optical fibers based on shape-memory polymers. *Nat. Commun.* **14**, 6561 (2023).
57. Zhang, J. et al. Crystal modifications and thermal behavior of poly(l-lactic acid) revealed by infrared spectroscopy. *Macromolecules* **38**, 8012–8021 (2005).
58. Echeverría, C., Limón, I., Muñoz-Bonilla, A., Fernández-García, M. & López, D. Development of highly crystalline polylactic acid with β-crystalline phase from the induced alignment of electrospun fibers. *Polymers* **13**, 2860 (2021).
59. Jokar, M., Abdul Rahman, R., Ibrahim, N. A., Abdullah, L. C. & Tan, C. P. Melt production and antimicrobial efficiency of low-density polyethylene (LDPE)-silver nanocomposite film. *Food Bioprocess Technol.* **5**, 719–728 (2012).
60. Yang, H., Jacucci, G., Schertel, L. & Vignolini, S. Cellulose-based scattering enhancers for light management applications. *ACS Nano* **16**, 7373–7379 (2022).
61. Reddy, I. V. A. K. et al. Ultrabroadband terahertz-band communications with self-healing Bessel beams. *Commun. Eng.* **2**, 1–9 (2023).
62. Hutchinson, M. H., Dorgan, J. R., Knauss, D. M. & Hait, S. B. Optical properties of polylactides. *J. Polym. Environ.* **14**, 119–124 (2006).
63. Ward, C. P. & Reddy, C. M. We need better data about the environmental persistence of plastic goods. *Proc. Natl. Acad. Sci.* **117**, 14618–14621 (2020).
64. Wurzbacher, C. E. et al. Planctoellipticum variicoloris gen. nov., sp. nov., a novel member of the family Planctomycetaceae isolated from wastewater of the aeration lagoon of a sugar processing plant in Northern Germany. *Sci. Rep.* **14**, 5741 (2024).
65. Boedeker, C. et al. Determining the bacterial cell biology of Planctomycetes. *Nat. Commun.* **8**, 14853 (2017).
66. Wang, L. et al. Review on Nonconventional Fibrillation Methods of Producing Cellulose Nanofibrils and Their Applications. *Biomacromolecules* **22**, 4037–4059 (2021).
67. Delgado-Aguilar, M. et al. Approaching a Low-Cost Production of Cellulose Nanofibers for Papermaking Applications. *BioResources* **10**, 5345–5355 (2015).
68. Wellenreuther, C., Wolf, A. & Zander, N. Cost competitiveness of sustainable bioplastic feedstocks – A Monte Carlo analysis for polylactic acid. *Clean. Eng. Technol.* **6**, 100411 (2022).
69. Wimberger, L., Ng, G. & Boyer, C. Light-driven polymer recycling to monomers and small molecules. *Nat. Commun.* **15**, 2510 (2024).
70. US polyethylene price evolution and what to expect | McKinsey. https://www.mckinsey.com/industries/chemicals/our-insights/us-polyethylene-price-evolution-and-what-to-expect.
71. Liu, W., Wu, X., Chen, X., Liu, S. & Zhang, C. Flexibly Controlling the Polycrystallinity and Improving the Foaming Behavior of Polylactic Acid via Three Strategies. *ACS Omega* **7**, 6248–6260 (2022).
72. Segal, L., Creely, J. J., Martin, A. E. & Conrad, C. M. An empirical method for estimating the degree of crystallinity of native cellulose using the X-ray diffractometer. *Text. Res. J.* **29**, 786–794 (1959).

Acknowledgements

The authors thank the Institute of Materials Science and Engineering, and the Chemical and Environmental Analysis Facility for their aid and facility access. P.S.D. also gratefully acknowledges support by the McDonnell International Scholars Academy. This work was supported by NSF EEC 2330245 and NSF MCB 2229160 from J.S.Y and S.Y.D and U.S. Department of Energy Project DE EE 0009756 from J.S.Y and S.Y.D.

Author contributions

J.S.Y. conceptualized the project. P.S.D., A.H., C.H., S.Y.D., and J.S.Y. developed the methodology. P.S.D., A.H., C.H., S.Y.D., and J.S.Y. carried out the experiments. P.S.D., A.H., C.H., and V.H. wrote and edited this work. S.Y.D. and J.S.Y. acquired the funding.

Competing interests

The authors declare no competing interests in the development of this work.

Additional information

Supplementary information The online version contains supplementary material available at https://doi.org/10.1038/s41467-025-61693-2.

Correspondence and requests for materials should be addressed to Joshua S. Yuan.

Peer review information *Nature Communications* thanks Dong Xie, Junyong Zhu and the other, anonymous, reviewer(s) for their contribution to the peer review of this work. A peer review file is available.